Eco-Environment & Health 3 (2024) 137–144

Contents lists available at ScienceDirect

Eco-Environment & Health

journal homepage: www.journals.elsevier.com/eco-environment-and-health

Original Research Article

Surface property and *in vitro* toxicity effect of insoluble particles given by protein corona: Implication for PM cytotoxicity assessment

Sisi Chen [a], Yexuan Zhang [a], Hongjuan Chen [b], Weijuan Zheng [b], Xin Hu [a], Li Mao [c], Xuewen Guo [a], Hongzhen Lian [a,*]

[a] State Key Laboratory of Analytical Chemistry for Life Science, School of Chemistry & Chemical Engineering and Center of Materials Analysis, Nanjing University, Nanjing 210023, China
[b] State Key Laboratory of Pharmaceutical Biotechnology, School of Life Science, Nanjing University, Nanjing 210023, China
[c] Ministry of Education (MOE) Key Laboratory of Modern Toxicology, School of Public Health, Nanjing Medical University, Nanjing 211166, China

ARTICLE INFO

Keywords:
Atmospheric particulate matter
Insoluble particles
Protein corona
Cytotoxicity
Proteomics

ABSTRACT

In vitro toxicological assessment helps explore key fractions of particulate matter (PM) in association with the toxic mechanism. Previous studies mainly discussed the toxicity effects of the water-soluble and organic-soluble fractions of PM. However, the toxicity of insoluble fractions is relatively poorly understood, and the adsorption of proteins is rarely considered. In this work, the formation of protein corona on the surface of insoluble particles during incubation in a culture medium was investigated. It was found that highly abundant proteins in fetal bovine serum were the main components of the protein corona. The adsorbed proteins increased the dispersion stability of insoluble particles. Meanwhile, the leaching concentrations of some metal elements (e.g., Cu, Zn, and Pb) from PM increased in the presence of proteins. The toxicity effects and potential mechanisms of the PM insoluble particle–protein corona complex on macrophage cells RAW264.7 were discussed. The results revealed that the PM insoluble particle–protein corona complex could influence the phagosome pathway in RAW264.7 cells. Thus, it promoted the intracellular reactive oxygen species generation and induced a greater degree of cell differentiation, significantly altering cell morphology. Consequently, this work sheds new light on the combination of insoluble particles and protein corona in terms of PM cytotoxicity assessment.

1. Introduction

Numerous epidemiological studies have indicated that atmospheric particulate matter (PM) is associated with the development of a range of respiratory, cardiovascular, and neurological diseases [1–4]. Until now, the specific toxicity mechanisms of PM remain unclear. This is due in large part to the fact that PM is a heterogeneous mixture. It consists of (i) water-soluble components, mainly inorganic salts and water-soluble organic compounds (WSOC) [5]; (ii) organic-soluble components, including polycyclic aromatic hydrocarbons (PAHs), long-chain alkanes, patchouli alkanes, etc. [6,7]; and (iii) insoluble fractions, mainly carbonaceous particles, natural and artificial mineral particles (e.g. insoluble silicates and metal oxides), and engineered nanoparticles (NPs) from anthropogenic emissions [8,9]. Previous studies mostly focused on the toxicity effects of water-soluble or organic-soluble fractions of PM [10–12]. However, the toxicity of insoluble fractions of PM cannot be ignored [13–15]. Some relevant studies have pointed out that the insoluble fraction of PM might cause more severe cell damage. For example, it might induce lower cell viability [16], higher levels of reactive oxygen species (ROS) [5,14], and more significant DNA damage [17]. On the other hand, there is growing evidence showing that tiny particles of PM can penetrate biological barriers and be distributed within several organs of the body, such as blood, cerebrospinal fluid, and bone joints [18–21]. When these particles enter the physiological body fluids, they will encounter various biomolecules, especially large amounts of proteins.

The concept of protein corona was first proposed in 2007 to describe the phenomenon of protein self-assembly on the surface of NPs to form protein layers [22]. In general, any nano- or microparticles exposed to physiological fluids will interact with biological macromolecules, including proteins [23]. The formation of protein corona not only changes the size, aggregation state, and interfacial properties of NPs [24–26] but also imparts new biological properties to NPs. This directly affects various responses of NPs in organisms, such as cellular uptake,

* Corresponding author.
E-mail address: hzlian@nju.edu.cn (H. Lian).

https://doi.org/10.1016/j.eehl.2024.01.011
Received 11 October 2023; Received in revised form 18 January 2024; Accepted 25 January 2024
Available online 28 February 2024

clearance rate, immune interference, and pro-inflammatory effects. [27–31].

Although research on the protein corona of engineered NPs has become popular in the past decade, limited data are available on the protein corona of PM. Recently, two *ex vivo* studies pointed out that PM binding to certain specific proteins could activate the protein's activity, and then trigger cascade reactions [32], or disrupt the interstitial extracellular matrix [33]. In addition, a few studies discussed the effects of protein corona on PM toxicity. Song's group found that fibrinogen-decorated $PM_{2.5}$ could reduce $PM_{2.5}$-induced oxidative stress and particulate uptake by RAW264.7 cells [34]. Li et al. found that human serum-derived protein corona on $PM_{2.5}$ could reduce the physical interaction of $PM_{2.5}$ with cell membranes but at the same time induce abnormal proliferation of human lung fibroblasts [35]. There is no doubt that the new surface properties conferred to PM by the bound protein corona would influence its toxicity effects. However, the adsorption of proteins during incubation has rarely been taken into account in current *in vitro* toxicity assessments, which may underestimate or overestimate the toxicity of insoluble fractions of PM. Moreover, further understanding of the role of protein corona in PM toxicity at the proteomic level is still lacking.

Herein, we focused on the formation of protein corona upon incubation of PM with fetal bovine serum (FBS) in cell culture medium during *in vitro* exposure. The composition of the protein corona and surface properties of particles were characterized. At the same time, we further compared the leaching of heavy metal elements from PM in the presence or absence of FBS. Mouse macrophage cell line RAW264.7 was employed to assess the cytotoxicity attribution of insoluble particles in PM, focusing especially on the effect of insoluble particles–protein corona complex. Finally, iTRAQ quantitative proteomics analysis was used to investigate the differentially expressed proteins (DEPs) and the enriched pathways in the exposed cells to provide more clues to elucidate the toxicity mechanism of insoluble particles and insoluble particles–protein corona complexes.

2. Materials and methods

2.1. Standard PM reference material

PM (Standard reference material 1648a) was purchased from the National Institute of Standards and Technology (NIST, USA). The characteristics of the PM with respect to size, morphology, and chemical properties are described in detail in Supplementary Text S1.1.

2.2. PM insoluble particle–protein corona complex preparation

The PM was incubated with different FBS concentrations (10%, 50%) at 37 °C for 24 h. The FBS solutions were diluted with high-glucose Dulbecco's modified eagle medium (DMEM) to keep the final PM concentration at 1 mg/mL. To obtain the PM insoluble particle–protein corona complex, the suspensions were centrifuged at 8,000 rpm for 10 min and the precipitates were subsequently washed three times with phosphate buffered saline (PBS) to remove the unadsorbed proteins. Meanwhile, the control sample was prepared in DMEM without FBS, and the rest of the steps were the same as above. A scheme of the PM insoluble particle–protein corona complex preparation procedures is shown in Fig. S1. To facilitate description, "PM-0% FBS", "PM-10% FBS", and "PM-50% FBS" were used in the following text.

2.3. Characterization of PM insoluble particle–protein corona complex

The functional groups on the surface of PM insoluble particle–protein corona complexes were characterized by an attenuated total reflection-Fourier transform infrared (ATR-FTIR) spectrometer (Nicolet iS10, ThermoFisher Scientific, USA). For characterizing the size and morphology of PM insoluble particle–protein corona complexes by scanning electron microscopy-energy dispersive X-ray spectroscopy (SEM-EDX) (S-4800, Hitachi, Japan), the obtained particles were suspended in water and then dropped onto silicon wafers. The hydrodynamic diameters of PM insoluble particle–protein corona complexes in PBS were measured by dynamic light scattering (DLS) (90 Plus, Brookhaven, USA), and the zeta potential values of their dispersion solutions were analyzed by a zetasizer (Nano-Z, Malvern, UK).

2.4. Characterization of protein corona compositions

The proteins adsorbed on the surface of insoluble matters were eluted according to previous literature [36]. First, 2 mL 8 M urea containing 2% 3-[(3-Cholamidopropyl)dimethylammonio]-1-propanesulfonate hydrate was added to each sample and then vortexed thoroughly and sonicated to extract the proteins. After centrifugation, the supernatant was recovered. Then prechilled acetone was added and left overnight at −20 °C to allow the proteins to precipitate completely. The proteins were redissolved in 8 M urea for SDS-PAGE and liquid chromatography-mass spectrometry/mass spectrometry (LC-MS/MS) analyses. Details are described in Supplementary Text S1.2.

2.5. Determination of metal elements release from PM

The effect on the release of metal elements from PM in the presence of protein *in vitro* was determined. Similarly, PM was suspended in PBS with or without 10% FBS at a concentration of 1 mg/mL and then incubated at 37 °C for 24 h. After centrifugation, the supernatants were collected.

Subsequently, the precipitates obtained from the above centrifugation were washed, centrifuged, and then re-dispersed in PBS. Likewise, the redispersed samples were incubated at 37 °C for another 24 h. After centrifugation, the supernatants were also collected.

All the respective collected supernatants were diluted 10 times with 1% dilute HNO_3. The concentration of metal elements was determined by NexION 350D ICP-MS (PerkinElmer, USA). The blank PBS solution and the PBS containing 10% FBS were also measured. A scheme of the released metal elements analysis is shown in Fig. S2.

2.6. Cell culture

RAW264.7 cells were cultured in high glucose DMEM supplemented with 10% FBS at 37 °C under 5% CO_2.

2.7. Preparation of PM samples for in vitro exposure

Since RAW264.7 cells were generally cultured in DMEM medium containing 10% FBS, this concentration was selected for incubating the protein corona for toxicity studies. The PM samples were prepared as follows. PM-insoluble particles–protein corona (PM-IP-corona) samples: PM was dispersed in DMEM medium containing 10% FBS at a concentration of 1 mg/mL. After 4 h of incubation at 37 °C, the PM suspension was centrifuged and the supernatant was discarded. Then the insoluble fraction of PM was washed with PBS to remove the unadsorbed proteins. Finally, an equal volume of DMEM medium without FBS was added to disperse the insoluble particles. PM-insoluble particles (PM-IP) samples: PM was first dispersed in DMEM medium without FBS at a concentration of 1 mg/mL, followed by incubation, centrifugation, and washing steps. Finally, the insoluble particles were resuspended in DMEM medium without FBS, representing the insoluble particles that did not form a protein corona. PM-water-soluble fraction (PM-WS) samples: PM was dispersed with DMEM medium without FBS after incubation, and the supernatant was separated and removed to a new tube. For the convenience of description, the concentration of the PM-WS mother liquid was also considered as 1 mg/mL. PM suspension (PM-S) samples: PM was directly dispersed in DMEM medium without FBS, representing a mixed fraction of water-soluble fraction and insoluble fraction which did not form the protein corona.

2.8. Cell viability assay

Cell viability of RAW264.7 cells after exposure to PM-IP-corona, PM-IP, PM-WS, and PM-S was determined by the cell counting kit-8 (CCK-8) (Beyotime, China). Details are described in Supplementary Text S1.3.

2.9. Intracellular ROS measurement

Intracellular ROS levels of RAW264.7 cells after exposure to PM-IP-corona, PM-IP, PM-WS, and PM-S were measured using a 2,7-dichlorodihydrofluorescein diacetate (DCFH-DA) fluorescent probe (Beyotime, China). Details are described in Supplementary Text S1.4.

2.10. Cell lysate extraction and iTRAQ labeling

To analyze the protein expression levels, lysates of RAW264.7 cells after exposure to 200 μg/mL PM-IP-corona, PM-IP, and PM-S were prepared and the proteins were alkylated, trypsin-digested, and labeled with the iTRAQ reagent-8 plex multiplex kit (AB Sciex, USA) based on our previous work [37,38]. Finally, the labeled samples were analyzed by the Nano LC-Triple TOF 5600+ system (AB Sciex, USA). Details are described in Supplementary Text S1.5.

2.11. Immunofluorescence analysis of F4/80 and CD68

Expressions of F4/80 and CD68 in RAW264.7 cells after exposure to PM-IP and PM-IP-corona were characterized by immunofluorescence imaging. Details are described in Supplementary Text S1.6.

2.12. Cell morphology by transmission electron microscope (TEM)

RAW264.7 cells were plated in 10-cm dishes at a density of 1×10^6 cells/mL. After being cultured for 24 h, the culture medium was discarded and 200 μg/mL PM-IP-corona or fresh DMEM medium was added. After a 24 h exposure, the cells were harvested followed by soaking in an electron microscope fixative. After embedding in resin, the cell sections were imaged by TEM (HT 7800, Hitachi, Japan).

2.13. Statistics and bioinformatics

The results were expressed as means ± standard deviations (SD). All the measurements were conducted at least twice, with at least three replicates per group. One-way analysis of variance (ANOVA) was employed to determine significant differences between the treatment groups and control groups in the cytotoxicity tests. Statistically significant differences were signed with *: $P < 0.05$, **: $P < 0.01$, and ***: $P < 0.001$.

The ProteinPilot™ software version 4.2 (AB Sciex, USA) was adopted for protein identification. Meanwhile, the MaxQuant software version 1.5.3.17 was adopted to obtain a label-free quantification for the relative percentages (%) of proteins in the corresponding corona samples, which were incubated with different serum concentrations. Intensity-based absolute quantification (iBAQ) was calculated to represent the relative protein amounts within the group [39]. Bioinformatics based on iTRAQ quantification for Kyoto Encyclopedia of Genes and Genomes (KEGG) pathway and Gene Ontology (GO) annotation analyses were referred to in our previous work [37,38]. Details are described in Supplementary Text S1.7.

3. Results and discussion

3.1. Protein corona formation on the surface of insoluble particles in PM

Protein corona could be classified as “hard” corona and “soft” corona. The hard corona was the protein layer with higher binding affinity to the particles, while the soft corona was the weaker bound protein layer formed in the outer layer of the hard corona, where the bound protein could be replaced by molecules with higher affinity [40]. Herein, the hard corona on the surface of insoluble particles in PM was studied, as the unbound or weakly bound proteins were removed by washing and centrifugation.

Using ATR-FTIR, significant amounts of amide functional group were found on the insoluble particles' surface, indicating the formation of protein corona on the surface of the particles. As shown in Fig. 1A, after incubation with 10% FBS and 50% FBS, three distinct peaks at 3,286, 1,532, and 1,398 cm^{-1} were generated, where the peaks at 3,286 and 1,532 cm^{-1} could be attributed to the stretching and bending vibration of

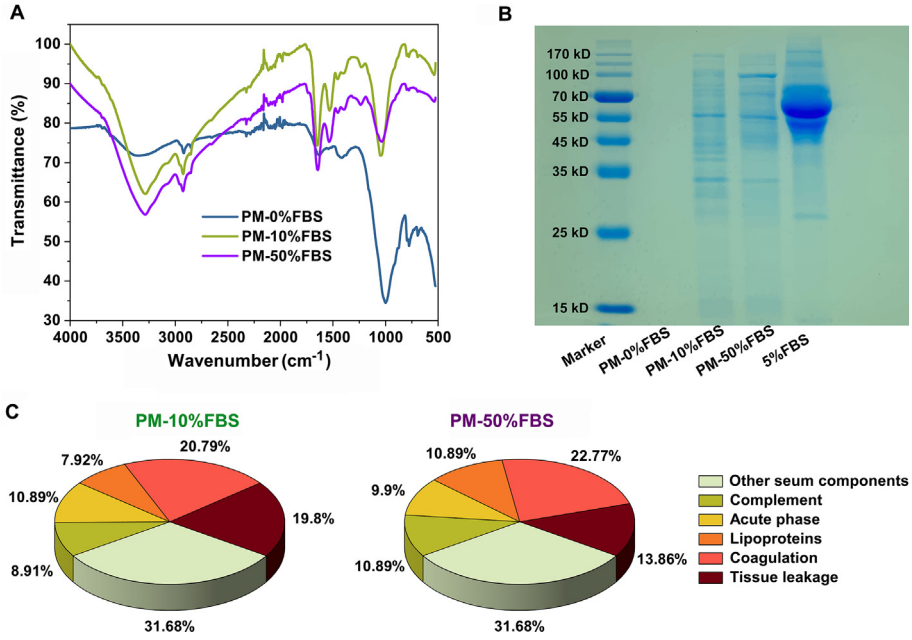

Fig. 1. ATR-FTIR spectra of PM-insoluble particles after incubation with 0%, 10%, and 50% FBS (A). SDS-PAGE analysis of the proteins adsorbed on the surface of the insoluble particles (B). Classification of the protein corona components in accordance with their functions (C).

N–H in –CO–NH–, and the peak at 1,398 cm^{-1} could be attributed to the stretching vibration of C–N in –CO–NH–. Moreover, the peak at 1,651 cm^{-1} showed a sharp increase, likely corresponding to the stretching vibration of C=O in –CO–NH–. Additionally, the spectral transmittances of the stretching vibration peak of Si–O–Si at 1,100 cm^{-1} and the symmetric stretching vibration peak of Si–O at 800 cm^{-1} were reduced after incubation with 10% FBS and 50% FBS, which might also be due to the proteins on the surface of silicate or silica particles in the PM.

The compositions of the protein coronas were identified by LC-MS/MS (Tables S1 and S2). Albumin, apolipoproteins (such as ApoA-I, ApoA-II, ApoE), and hemoglobin were the main compositions of the protein coronas of the insoluble particles, which had also been found to have a strong affinity to the different NPs [41–43], as these proteins were in high abundance in the serum. Interestingly, some low-abundant proteins were also adsorbed to the particles' surface when incubated with 10% FBS; and when the concentration of FBS was increased to 50%, the protein file of the protein corona changed, as well as the relative percentages of the proteins within the group (Fig. S3). The SDS-PAGE additionally exhibited the distribution of the protein bands (Fig. 1B). It indicated that in addition to being influenced by the protein concentration in the biological environment, there were other driving forces between the insoluble particles and proteins that led to competitive adsorption, whereby proteins with lower binding affinities were replaced by that with higher binding affinities showing a decrease in adsorption [44]. Moreover, the proteins were classified according to their functions (Fig. 1C). There were a variety of coagulation-related proteases and protease inhibitors in serum binding to the insoluble particles, such as serine protease 1, plasminogen, prothrombin, alpha-2-antiplasmin, coagulation factor V. The interaction between particles and proteins would disturb protein conformation and affect protein activity. Previously, Jin et al. found that $PM_{2.5}$ could bind with Hageman factor XII and cause its autoactivation, which further triggered a series of cascade activation of the kallikrein–kinin system, thereby promoting hematotoxicity [32]. Therefore, the fact of the interaction between airborne insoluble particles and coagulation-related proteins could provide clues for the assessment the PM toxicity to the cardiovascular system. Moreover, high-density lipoproteins (ApoA-I, ApoA-II, ApoE) were found to have a high coverage of the protein coronas (Table S3), while in terms of low-density lipoproteins, for example, ApoB was virtually absent (0.02% in PM-10% FBS, and 0.001% in PM-50% FBS, as calculated from the relative intensities of iBAQ). Previous studies demonstrated that high-density lipoproteins could influence cellular uptake, however, which apolipoproteins played a major role varied in different situations [44–46]. In general, our findings serve as valuable clues for further studies focusing on the role of specific proteins in protein corona–cell interactions.

3.2. *Effect of proteins on the surface properties and release of metal elements from PM*

First, the morphologies of the PM-insoluble particles after incubation with 0%, 10%, and 50% FBS were characterized, with particle sizes ranging from several hundred nanometers to a few micrometers (Fig. 2A). No observable differences were detected among the particles treated with and without FBS. It revealed that the thickness of the protein corona layer was much smaller compared to the size of these particles. Nevertheless, herein, the distribution of S element on the surface of the insoluble particle after incubation with FBS was observed by EDX for the first time (Fig. S4), which should be attributed to the sulfur-containing amino acids (mainly cysteine and methionine residues) in the proteins. It provided evidence for the formation of the protein corona on the surface of PM-insoluble particles.

The stability of particles can be increased by adsorbing proteins that change hydrophilicity and surface charge [25], and here we also found that the protein corona increased the dispersion stability of PM-insoluble particles. As shown in Fig. 2B, the distributions of insoluble particles with hydrodynamic diameters around 300 nm were increased after incubation with FBS, which might be attributed to the presence of protein corona promoting the stability of these nanoparticles and reducing aggregation. In addition, it was found that the insoluble particles were less likely to settle after being decorated with proteins (Fig. S5). The zeta potential of

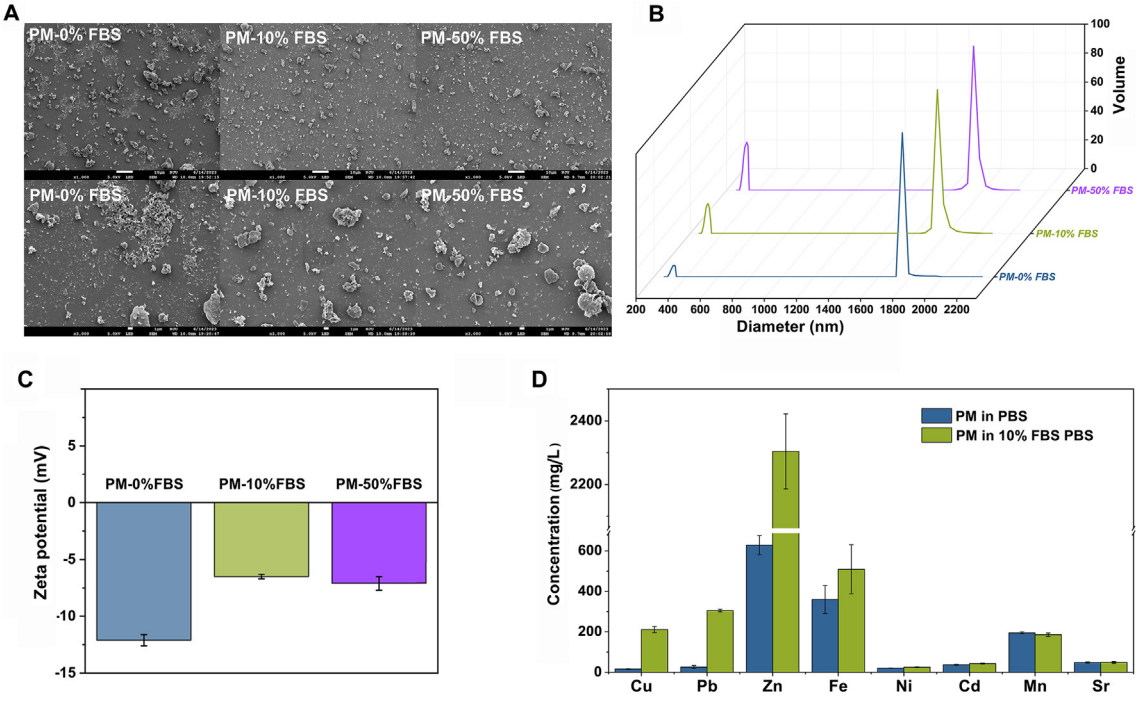

Fig. 2. SEM images of PM-insoluble particles after incubation with 0%, 10%, and 50% FBS (A). Multimodal size distributions of PM-insoluble particles after incubation with 0%, 10%, and 50% FBS by DLS measurements (B). Zeta potential of PM-insoluble particles after incubation with 0%, 10%, and 50% FBS (C). Concentrations (mg/L) of main metal elements from PM when incubated in PBS and 10% FBS PBS (D).

the insoluble particles incubated without FBS exhibited a negative surface charge, while decoration with proteins increased the zeta potential (Fig. 2C). No distinct difference in the zeta potential was observed between PM-10% FBS and PM-50% FBS samples, possibly due to the saturation of the adsorption sites of the particles after incubation with both 10% FBS and 50% FBS.

Moreover, considering that the solubility of PM-bound metals can be affected by serum proteins in the *in vitro* test, as demonstrated by previous works where adding specific proteins to simulated body fluids would affect the bioavailability of metal elements in PM [47,48], we then determined the concentrations of metal elements released from PM when incubated with or without FBS. In the presence of proteins, the concentrations of Cu, Zn, and Pb increased significantly, and the concentrations of Fe and Ni increased slightly, while there were no changes in the concentrations of Mn, Sr, and Cd (Fig. 2D). This might be attributed to the coordination of metal ions with proteins, along with the possible contributions of metalloproteins presented in the serum. In turn, protein-metal ion interactions might alter protein activity and affect protein stability.

To minimize possible interference with subsequent toxicity analysis due to the differences in metal elements dissolution, we determined and compared the concentrations of metal elements leached from the above obtained insoluble particles-protein corona complex and insoluble particles without the protein corona after redispersed in PBS (Table S4). The concentrations of the metal elements were all reduced by three orders of magnitude, and the concentrations of the metal elements from the insoluble particles–protein corona complex were comparable to those from the insoluble particles without the protein corona. Thus, in subsequent toxicity studies, the effect of metal element releaching on the toxicity of insoluble particles could be disregarded, and the effect of the difference in toxicity could be considered only in terms of whether the insoluble particles in PM form protein coronas or not.

3.3. The cytotoxicity induced by PM-IP and PM-IP-corona compared to PM-WS and PM-S

The differences in cytotoxicity of PM-IP, PM-IP-corona, PM-WS, and PM-S to RAW264.7 cells were compared. The viability of RAW264.7 cells was significantly increased by PM-IP and PM-IP-corona at low concentrations, followed by a decrease in cell viability at higher doses (Fig. 3A). This suggested that the insoluble particles in PM could promote RAW264.7 cells proliferation regardless of whether they form a protein corona or not. This might reflect an adaptive response of cells to external stimuli and a regulation of the cell cycle by RAW264.7 cells in a serum-starved state (for avoiding re-adsorption of proteins by the insoluble particles during exposure) to prevent apoptosis or involving oxidative stress process. For example, Bayram et al. previously found that low-dose diesel exhaust particle exposure could reverse serum starvation-induced quiescence of lung epithelial cells A549 in the G0 phase, promoting cell proliferation and reducing apoptosis [49]. Moreover, the formation of the protein corona by insoluble particles did not seem to reduce the toxicity of the particles, as evidenced by the lower cell viability of the PM-IP-corona group compared to that of the PM-IP group at the same concentration. Similarly, when exposed to PM-WS, the viability of cells increased slightly at relatively low concentrations and then decreased slightly, but the effect was not significant. Furthermore, the viability of cells was significantly decreased in a dose-dependent manner after exposure to PM-S for 24 h. This indicated potential synergistic effects between the insoluble particles and water-soluble components of PM, resulting in the highest cytotoxicity of PM-S.

The intracellular ROS levels affected by the four PM stimulants were determined, which were expressed as fold changes of DCFH-DA fluorescence intensities relative to the control group. The intracellular ROS levels in RAW264.7 cells of the four groups increased significantly in a dose-dependent manner, where PM-IP-corona and PM-S induced a

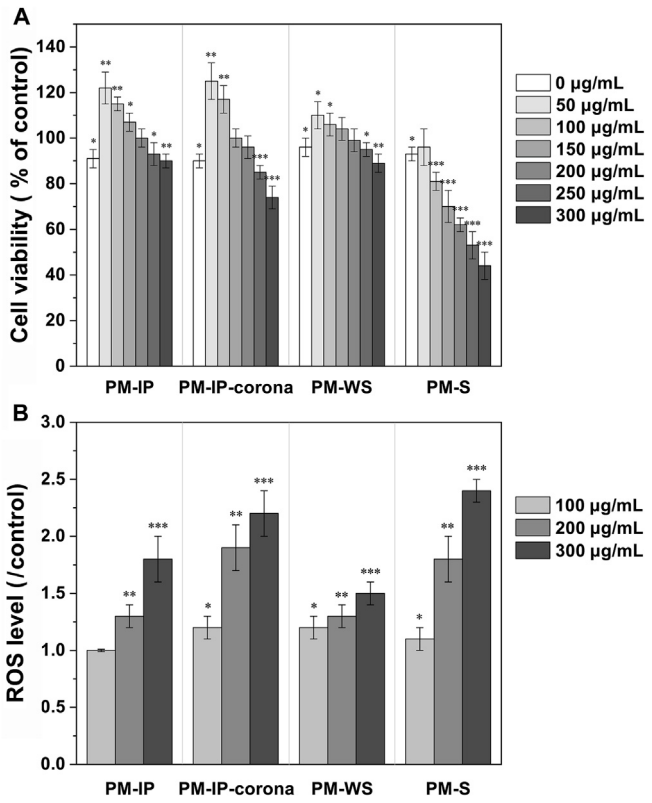

Fig. 3. Cell viabilities (A) and intracellular ROS levels (B) of RAW264.7 cells after exposure to PM-IP, PM-IP-corona, PM-WS, and PM-S for 24 h.

comparable increase in intracellular ROS levels, while PM-WS caused relatively less ROS generation (Fig. 3B). Combined with the results of cell viability, it seemed that the cytotoxicity of insoluble particles was associated with oxidative stress and that RAW264.7 cells could resist oxidative stress through defense mechanisms and promote cell proliferation under the stress of particles at low concentrations. However, when particle accumulation exceeded cellular clearance capacity, RAW264.7 cells, as macrophages, could phagocytose exogenous particles [50], and then induce a substantial ROS generation, triggering the production of inflammatory factors [51], finally resulting in cellular damage or apoptosis. In addition, the formation of the protein corona by insoluble particles in PM increased the oxidative stress in cells. Especially at 200 μg/mL, the ROS level of RAW264.7 cells induced by PM-IP-corona was much higher than that induced by PM-IP. It was possibly due to the enhanced cellular uptake of protein-decorated particles by RAW264.7 cells, which will be considered in detail later.

3.4. Potential pathways affected by PM-IP, PM-IP-corona and PM-S

To elucidate the mechanisms underlying the differences in cytotoxicity, the toxicological proteomics of RAW264.7 cells after exposure to PM-IP, PM-IP-corona, and PM-S were analyzed. A total of 2,754 proteins were identified based on iTRAQ quantitative proteomics. Of these proteins, 103, 111, and 94 DEPs were selected in the PM-IP, PM-IP-corona, and PM-S groups, respectively (the details of the DEPs are listed in Tables S4-6). GO annotations of these DEPs were analyzed (Tables S8-16), and Fig. S6-8 represent the top 15 significantly enriched GO terms. In general, there were a great number of proteins related to protein synthesis and transport, redox reactions, DNA damage responses, cell proliferation, and apoptosis affected by PM-IP, PM-IP-corona, and PM-S. In addition, there were special concerns associated with the most significantly enriched biological process, cell differentiation. Previous studies also reported that RAW264.7 cells could differentiate towards more differentiated anti-inflammatory

macrophages upon stimulation, with ROS and pro-inflammatory factors playing a key role, as evidenced by increased cell size, elongated spindle shape, significantly increased cell membrane roughness and enhanced cell adhesion [52–54]. The results of the GO analysis in this present work showed similar biological processes involved in the DEPs induced by the three stimuli, which implied that the toxicity of insoluble particles in PM could not be negligible.

Meanwhile, the KEGG pathways enriched by DEPs in RAW264.7 cells affected by PM-IP, PM-IP-corona, and PM-S were analyzed (Fig. 4). There were five common pathways shared by three groups, including "systemic lupus erythematosus", "alcoholism", "neutrophil extracellular trap formation", "viral carcinogenesis", and "protein processing in endoplasmic reticulum". It indicated that PM-IP, PM-IP-corona, and PM-S samples all induced the cellular immune response and inflammatory response in RAW264.7 cells.

In addition to the above five common pathways, in RAW264.7 cells exposed to PM-IP-corona, "aminoacyl-tRNA biosynthesis", "carbon metabolism", "glutathione metabolism", and "pentose and glucuronate interconversions" pathways were affected, all related to metabolic processes of the cells. In particular, the "phagosome" signaling pathway was also enriched by DEPs. The main mechanisms of particle uptake into cells include micropinocytosis, receptor-mediated endocytosis, phagocytosis, and diffusion or adhesive interactions [55]. Here, Fig. S9 represents a KEGG map of the phagosome pathway in RAW264.7 cells exposed to PM-IP-corona, with asterisks marking the DEPs in the pathway. In addition, Fig. S10 shows the fold changes and *P* values of the DEPs, including tubulin alpha chain, dynein light intermediate chain, integrin beta (ITGB2), V-type proton ATPase subunit C (Atp6v1c1), vacuolar proton pump subunit B (Atp6v1b2), calreticulin and neutrophil cytosl factor 1 (NCF1) in PM-IP-corona group. Specifically, the most significant change was observed in the tubulin alpha chain, which is important for microtubule movement and maintenance of the cytoskeleton. Yue et al. investigated the uptake of chitosan particles with different particle sizes (nano- and micro-) by J774A.1 macrophage cells, and the results showed that phagocytosis was an essential internalization mechanism for all the particles, and that microtubule movement was involved in the phagocytosis process, resulting in rearrangement of the actin cytoskeleton [56]. In addition, ITGB2, Atp6v1c1, Atp6v1b2, and NCF1 were not significantly affected in the PM-IP and PM-S groups (Fig. S10). ITGB2 is the first phagocytic integrin to be characterized, also known as complement receptor (CR3) or Mac-1, that mediates and allows the binding and clearance of particles [57,58]. Atp6v1c1 and Atp6v1b2 are components of the vacuolar ATPase (V-ATPase) complex; the former is necessary for the assembly of the V–ATPase complex, whereas the latter is directly responsible for ATP hydrolysis. The V–ATPase complex plays a vital part in endosomal and lysosomal acidification, which is required for receptor-mediated endocytosis [59,60]. Therefore, the up-regulation of subunit C and vacuolar proton pump subunit B might imply that the cells were more involved in endocytosis activity related to the removal of extracellular substances. NCF1, also known as p47-phox, is a regulatory subunit of phagocyte nicotinamide adenine dinucleotide phosphate (NADPH) oxidase 2 complex (NOX2) [61]. Previous works suggested that NCF1 phosphorylation was necessary for NADPH oxidase activation and thus promoted ROS generation [62]. It is also consistent with the result of the elevated ROS levels in RAW264.7 cells exposed to PM-IP-corona (Fig. 3B), suggesting a relationship between phagosome and ROS generation. In conclusion, it implied that the airborne insoluble particles with the protein corona could promote the cellular uptake of particles by RAW264.7 cells via phagocytosis and receptor-mediated endocytosis.

As for PM-S stimulation, additional pathways included "spliceosome," "apoptosis," "pentose and glucuronate conversion," and "microRNAs in cancer" that were enriched by DEPs. Spliceosomes play an essential role in regulating gene expressions, while microRNAs are small non-coding RNAs that can modulate gene expressions, as well as various signaling molecules [63,64]. This result illustrated that PM-S caused the most severe damage to RAW264.7 cells compared to PM-IP and PM-IP-corona, which was consistent with the results on cell viability. The soluble fraction of PM-S in concert with the insoluble particle fraction might induce higher levels of genotoxicity.

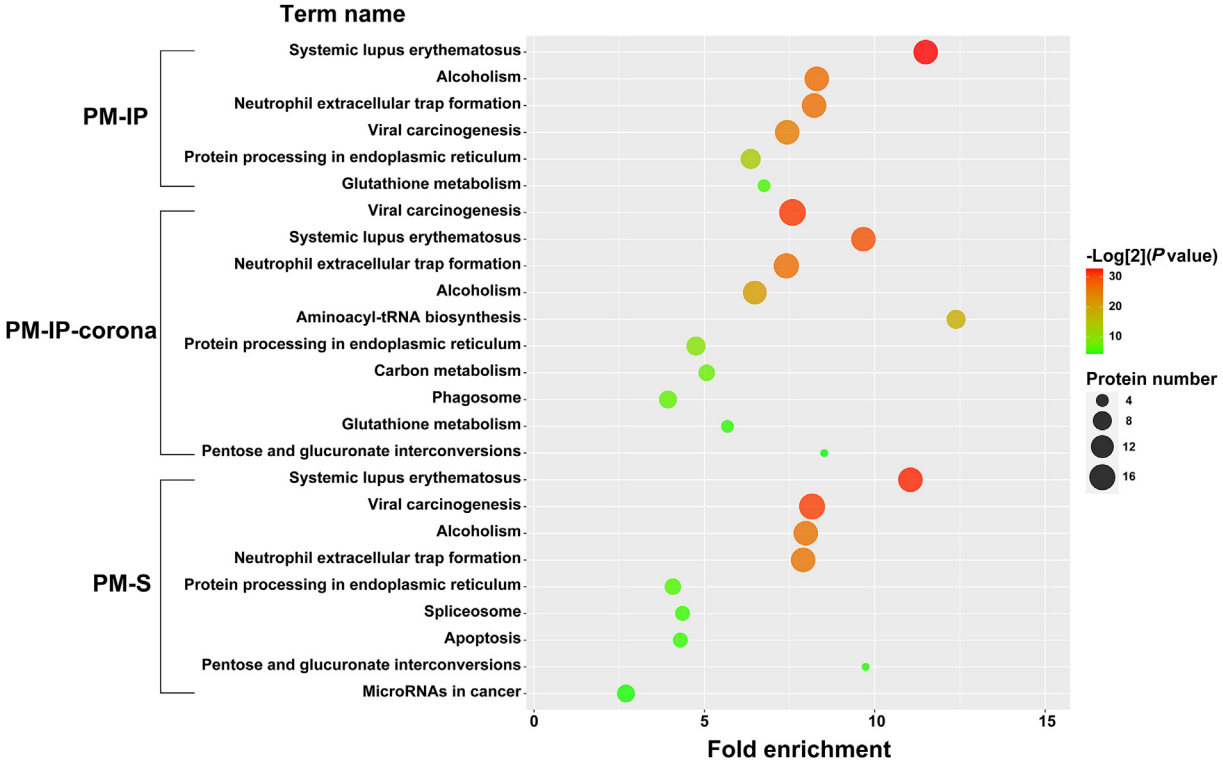

Fig. 4. KEGG pathways enriched by DEPs in RAW264.7 cells affected by PM-IP, PM-IP-corona, and PM-S.

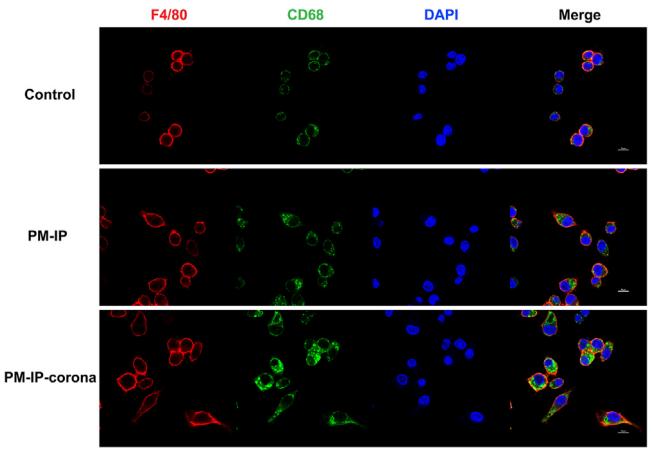

Fig. 5. Immunofluorescence confocal imaging of RAW264.7 cells after exposure to PM-IP and PM-IP-corona for 24 h.

3.5. *The morphology of RAW264.7 cells altered by PM-IP-corona*

The proteomics investigation revealed that the proteins related to cell differentiation and phagosome pathway were significantly affected in RAW264.7 cells exposed to PM-IP-corona. Therefore, to validate the proteomics results, the cell morphology was recorded. The localizations of F4/80, CD68 in RAW264.7 cells after exposure to PM-IP and PM-IP-corona were characterized by immunofluorescence (Fig. 5 and Fig. S11). F4/80 and CD68 are commonly used as biomarkers of macrophage activation, with F4/80 localized to the cell membrane [65], while CD68 localized to the cell membrane, endosomal membrane, and lysosomal membrane [66]. As shown in Fig. 5, the cells exposed to PM-IP-corona displayed an oval or irregular shape, as well as pseudopodia-like protrusions on the surface of the cells, compared to those exposed to PM-IP. Moreover, the average cell size was much larger in the PM-IP-corona group compared to the control group. It can be concluded that PM-IP-corona could induce a greater degree of differentiation of RAW264.7 cells compared to PM-IP, and although PM-IP-corona did not cause significant cell death, it obviously altered the cell morphology.

The flow cytometry method allows the quantification of cellular side scatter (SSC), reflecting changes in the refractive index of cytoplasmic structures [67]. The SSC intensity of RAW264.7 cells was enhanced with increasing particle concentrations, and the SSC intensity in the PM-IP-corona group was greater than that in the PM-IP and PM-S groups (Fig. S12 and S13). The internal cell structure was further imaged by TEM (Fig. S14). After exposure to PM-IP-corona, the nuclei of RAW264.7 cells appeared to be crinkled, mitochondria became swollen, and the number of intracellular lysosomes, phagosome, and cell vacuoles increased. This visually demonstrated that under PM-IP-corona exposure, RAW264.7 cells would phagocytose the granules and cause changes in the internal cell structure, inducing significant damage to the cells.

4. Conclusions

In this work, we discussed the impact of proteins in the culture medium on the assessment of PM toxicity during *in vitro* exposure. First, we found that the insoluble particles in PM can bind with proteins to form protein coronas, of which high-abundance proteins in FBS were the main components. Second, it was determined that in the presence of proteins, the soluble concentration of some metal elements in PM increased, particularly Cu, Zn, and Pb. Third, the formation of the protein corona from PM insoluble particles did not alleviate the toxicity to RAW264.7 cells, but instead promoted the production of intracellular ROS. The proteomics analysis further revealed that the phagosome pathway was significantly influenced by PM-insoluble particles with the protein corona, which induced a greater degree of cell differentiation and altered cell morphology. The relevance of the composition of the protein corona and the differentially expressed proteins on the phagosome pathway warrants more detailed investigation. Generally, these findings provide new insights into the complex cytotoxicity of PM combined with the protein corona, and more information on the effect of PM insolubility on the toxicity assessment.

CRediT authorship contribution statement

S.S.C.: conceptualization, investigation, methodology, formal analysis, visualization, data curation, writing–original draft. Y.X.Z.: formal analysis, visualization. H.J.C.: data curation, software. W.J.Z., X.H.: methodology, resources. L.M.: methodology, funding acquisition, resources. X.W.G.: methodology, formal analysis. H.Z.L.: conceptualization, methodology, funding acquisition, project administration, writing–review & editing.

Declaration of competing interests

The authors declare that they have no known competing financial interests or personal relationships that could have appeared to influence the work reported in this paper.

Acknowledgments

This work was supported by the National Natural Science Foundation of China (91643105, 21874065, 22176085).

Appendix A. Supplementary data

Supplementary data to this article can be found online at https://doi.org/10.1016/j.eehl.2024.01.011.

References

[1] G.B. Hamra, N. Guha, A. Cohen, F. Laden, O. Raaschou-Nielsen, J.M. Samet, et al., Outdoor particulate matter exposure and lung cancer: a systematic review and meta-analysis, Environ. Health Perspect. 122 (9) (2014) 906–911.
[2] P. Fu, X. Guo, F.M.H. Cheung, K.K.L. Yung, The association between $PM_{2.5}$ exposure and neurological disorders: a systematic review and meta-analysis, Sci. Total Environ. 655 (2019) 1240–1248.
[3] R.T. Burnett, C.A. Pope, M. Ezzati, C. Olives, S.S. Lim, S. Mehta, et al., An integrated risk function for estimating the global burden of disease attributable to ambient fine particulate matter exposure, Environ. Health Perspect. 122 (4) (2014) 397–403.
[4] M. Zhou, H. Wang, X. Zeng, P. Yin, J. Zhu, W. Chen, et al., Mortality, morbidity, and risk factors in China and its provinces, 1990–2017: a systematic analysis for the Global Burden of Disease Study 2017, Lancet 394 (10204) (2019) 1145–1158.
[5] L. Liu, Q. Zhou, X. Yang, G. Li, J. Zhang, X. Zhou, et al., Cytotoxicity of the soluble and insoluble fractions of atmospheric fine particulate matter, J. Environ. Sci. 91 (2020) 105–116.
[6] P.Q. Fu, K. Kawamura, C.M. Pavuluri, T. Swaminathan, J. Chen, Molecular characterization of urban organic aerosol in tropical India: contributions of primary emissions and secondary photooxidation, Atmos. Chem. Phys. 10 (2010) 2663–2689.
[7] G. Wang, K. Kawamura, S. Lee, K. Ho, J. Cao, Molecular, seasonal, and spatial distributions of organic aerosols from fourteen Chinese cities, Environ. Sci. Technol. 40 (15) (2006) 4619–4625.
[8] J.E. Thompson, Airborne particulate matter: human exposure and health effects, J. Occup. Environ. Med. 60 (5) (2018) 392–423.
[9] M.I. Setyawati, D. Singh, S.P.R. Krishnan, X. Huang, M. Wang, S. Jia, et al., Occupational inhalation exposures to nanoparticles at six Singapore printing centers, Environ. Sci. Technol. 54 (4) (2020) 2389–2400.
[10] Y. Lyu, S. Su, B. Wang, X. Zhu, X. Wang, E.Y. Zeng, et al., Seasonal and spatial variations in the chemical components and the cellular effects of particulate matter collected in Northern China, Sci. Total Environ. 627 (2018) 1627–1637.
[11] C. Roper, L.S. Delgado, D. Barrett, S.L.M. Simonich, R.L. Tanguay, $PM_{2.5}$ filter extraction methods: implications for chemical and toxicological analyses, Environ. Sci. Technol. 53 (1) (2019) 434–442.
[12] M. Pardo, F. Xu, M. Shemesh, X. Qiu, Y. Barak, T. Zhu, et al., Nrf 2 protects against diverse $PM_{2.5}$ components-induced mitochondrial oxidative damage in lung cells, Sci. Total Environ. 669 (2019) 303–313.

[13] N.Q. Vuong, D. Breznan, P. Goegan, J.S. O'Brien, A. Williams, S. Karthikeyan, et al., In vitro toxicoproteomic analysis of A549 human lung epithelial cells exposed to urban air particulate matter and its water-soluble and insoluble fractions, Part, Fibre Toxicol 14 (2017) 39.
[14] D. Wang, P. Pakbin, M.M. Shafer, D. Antkiewicz, J.J. Schauer, C. Sioutas, Macrophage reactive oxygen species activity of water-soluble and water-insoluble fractions of ambient coarse, $PM_{2.5}$ and ultrafine particulate matter (PM) in Los Angeles, Atmos. Environ. 77 (2013) 301–310.
[15] L. Massimi, M.L. Astolfi, S. Canepari, Simple and efficient method to detach intact PM_{10} from field filters: elements recovery assessment, Atmos. Pollut. Res. 13 (5) (2022) 101417.
[16] N.K. Gali, G. Li, Z. Ning, P. Brimblecombe, Diurnal trends in redox characteristics of water-soluble and -insoluble PM components, Environ. Pollut. 254 (2019) 112841.
[17] Z.H. Qi, Y.Y. Song, Q.Q. Ding, X.L. Liao, R.J. Li, G.G. Liu, et al., Water soluble and insoluble components of $PM_{2.5}$ and their functional cardiotoxicities on neonatal rat cardiomyocytes in vitro, Ecotoxicol. Environ. Saf. 168 (2019) 378–387.
[18] Y. Qi, S. Wei, Y. Chen, Y. Pu, S. Liu, Y. Liu, Intrusion of inhaled exotic ultrafine particles into the knee joint in humans and animals: a risk to the joint and surrounding tissues, Nano Today 43 (2022).
[19] W. Wang, Y. Lin, H. Yang, W. Ling, L. Liu, W. Zhang, et al., Internal exposure and distribution of airborne fine particles in the human body: methodology, current understandings, and research needs, Environ. Sci. Technol. 56 (11) (2022) 6857–6869.
[20] Y. Qi, S. Wei, T. Xin, C. Huang, Y. Pu, J. Ma, et al., Passage of exogeneous fine particles from the lung into the brain in humans and animals, Proc. Natl. Acad. Sci. U.S.A. 119 (26) (2022) e2117083119.
[21] D. Lu, Q. Luo, R. Chen, Y. Zhuansun, J. Jiang, W. Wang, et al., Chemical multi-fingerprinting of exogenous ultrafine particles in human serum and pleural effusion, Nat. Commun. 11 (1) (2020) 2567.
[22] T. Cedervall, I. Lynch, S. Lindman, T. Berggard, E. Thulin, H. Nilsson, et al., Understanding the nanoparticle-protein corona using methods to quantify exchange rates and affinities of proteins for nanoparticles, Proc. Natl. Acad. Sci. U.S.A. 104 (2007) 2050–2055.
[23] S. Lindman, I. Lynch, E. Thulin, H. Nilsson, K.A. Dawson, S. Linse, Systematic investigation of the thermodynamics of HSA adsorption to *N-iso*-propylacrylamide/*N-tert*-butylacrylamide copolymer nanoparticles. Effects of particle size and hydrophobicity, Nano Lett. 7 (2007) 914–920.
[24] J. Mo, Q. Xie, W. Wei, J. Zhao, Revealing the immune perturbation of black phosphorus nanomaterials to macrophages by understanding the protein corona, Nat. Commun. 9 (1) (2018) 2480.
[25] C. Moya, R. Escudero, D.C. Malaspina, M. de la Mata, J. Hernandez-Saz, J. Faraudo, et al., Insights into preformed human serum albumin corona on iron oxide nanoparticles: structure, effect of particle size, impact on MRI efficiency, and metabolization, ACS Appl. Bio Mater. 2 (7) (2019) 3084–3094.
[26] N. Liu, M. Tang, J. Ding, The interaction between nanoparticles-protein corona complex and cells and its toxic effect on cells, Chemosphere 245 (2020) 125624.
[27] A. Ghazaryan, K. Landfester, V. Mailander, Protein deglycosylation can drastically affect the cellular uptake, Nanoscale 11 (22) (2019) 10727–10737.
[28] R. Cai, J. Ren, Y. Ji, Y. Wang, Y. Liu, Z. Chen, et al., Corona of thorns: the surface chemistry-mediated protein corona perturbs the recognition and immune response of macrophages, ACS Appl. Mater. Interfaces 12 (2) (2020) 1997–2008.
[29] W. Hu, C. Peng, M. Lv, X. Li, Y. Zhang, N. Chen, C. Fan, Q. Huang, Protein corona-mediated mitigation of cytotoxicity of graphene oxide, ACS Nano 5 (2011) 3693–3700.
[30] S. Ritz, S. Schottler, N. Kotman, G. Baier, A. Musyanovych, J. Kuharev, et al., Protein corona of nanoparticles: distinct proteins regulate the cellular uptake, Biomacromolecules 16 (4) (2015) 1311–1321.
[31] G. Duan, S.G. Kang, X. Tian, J.A. Garate, L. Zhao, C. Ge, et al., Protein corona mitigates the cytotoxicity of graphene oxide by reducing its physical interaction with cell membrane, Nanoscale 7 (37) (2015) 15214–15224.
[32] X. Jin, Q. Ma, Z. Sun, X. Yang, Q. Zhou, G. Qu, et al., Airborne fine particles induce hematological effects through regulating the crosstalk of the kallikrein-kinin, complement, and coagulation systems, Environ. Sci. Technol. 53 (5) (2019) 2840–2851.
[33] Z. Wang, Z. Zhai, C. Chen, X. Tian, Z. Xing, P. Xing, et al., Air pollution particles hijack peroxidasin to disrupt immunosurveillance and promote lung cancer, Elife 11 (2022) e75345.
[34] Z. Liu, Q. Zhu, E. Song, Y. Song, Characterization of blood protein adsorption on $PM_{2.5}$ and its implications on cellular uptake and cytotoxicity of $PM_{2.5}$, J. Hazard Mater. 414 (2021) 125499.
[35] Y. Li, P. Wang, C. Hu, K. Wang, Q. Chang, L. Liu, et al., Protein corona of airborne nanoscale $PM_{2.5}$ induces aberrant proliferation of human lung fibroblasts based on a 3D organotypic culture, Sci. Rep. 8 (1) (2018) 1939.
[36] D. Docter, U. Distler, W. Storck, J. Kuharev, D. Wunsch, A. Hahlbrock, et al., Quantitative profiling of the protein coronas that form around nanoparticles, Nat. Protoc. 9 (9) (2014) 2030–2044.
[37] S.S. Chen, T.Q. Wang, W.C. Song, Z.J. Tang, Z.M. Cao, H.J. Chen, et al., A novel particulate matter sampling and cell exposure strategy based on agar membrane for cytotoxicity study, Chemosphere 300 (2022) 134473.
[38] Z.J. Tang, Z.M. Cao, X.W. Guo, H.J. Chen, Y. Lian, W.J. Zheng, et al., Cytotoxicity and toxicoproteomic analyses of human lung epithelial cells exposed to extracts of atmospheric particulate matters on PTFE filters using acetone and water, Ecotoxicol. Environ. Saf. 191 (2020) 110223.
[39] S. Tyanova, T. Temu, J. Cox, The MaxQuant computational platform for mass spectrometry-based shotgun proteomics, Nat. Protoc. 11 (12) (2016) 2301–2319.
[40] M.P. Monopoli, C. Aberg, A. Salvati, K.A. Dawson, Biomolecular coronas provide the biological identity of nanosized materials, Nat. Nanotechnol. 7 (12) (2012) 779–786.
[41] J. Simon, T. Wolf, K. Klein, K. Landfester, F.R. Wurm, V. Mailander, Hydrophilicity regulates the stealth properties of polyphosphoester-coated nanocarriers, Angew. Chem. Int. Ed. 57 (19) (2018) 5548–5553.
[42] Y. Ju, H.G. Kelly, L.F. Dagley, A. Reynaldi, T.E. Schlub, S.K. Spall, et al., Person-specific biomolecular coronas modulate nanoparticle interactions with immune cells in human blood, ACS Nano 14 (11) (2020) 15723–15737.
[43] S. Tenzer, D. Docter, S. Rosfa, A. Wlodarski, J. Kuharev, A. Rekik, et al., Nanoparticle size is a critical physico-chemical determinant of the human blood plasma corona: a comprehensive quantitative proteomic analysis, ACS Nano 5 (2011) 7155–7167.
[44] V. Castagnola, W. Zhao, L. Boselli, M.C. Lo Giudice, F. Meder, E. Polo, et al., Biological recognition of graphene nanoflakes, Nat. Commun. 9 (1) (2018) 1577.
[45] D. Chen, S. Ganesh, W. Wang, M. Amiji, The role of surface chemistry in serum protein corona-mediated cellular delivery and gene silencing with lipid nanoparticles, Nanoscale 11 (18) (2019) 8760–8775.
[46] O.E. Glukhova, T.R. Prytkova, G.V. Savostyanov, Simulation of high density lipoprotein behavior on a few layer graphene undergoing non-uniform mechanical load, J. Phys. Chem. B 120 (15) (2016) 3593–3600.
[47] B. Berlinger, D.G. Ellingsen, M. Naray, G. Zaray, Y. Thomassen, A study of the bio-accessibility of welding fumes, J. Environ. Monit. 10 (12) (2008) 1448–1453.
[48] B. Leclercq, L.Y. Alleman, E. Perdrix, V. Riffault, M. Happillon, A. Strecker, et al., Particulate metal bioaccessibility in physiological fluids and cell culture media: toxicological perspectives, Environ. Res. 156 (2017) 148–157.
[49] H. Bayram, K. Ito, R. Issa, M. Ito, M. Sukkar, K.F. Chung, Regulation of human lung epithelial cell numbers by diesel exhaust particles, Eur. Respir. J. 27 (4) (2006) 705–713.
[50] R. Su, X. Jin, W. Zhang, Z. Li, X. Liu, J. Ren, Particulate matter exposure induces the autophagy of macrophages via oxidative stress-mediated PI3K/AKT/mTOR pathway, Chemosphere 167 (2017) 444–453.
[51] F.F. Xu, X.H. Qiu, X.Y. Hu, Y. Shang, M. Pardo, Y.H. Fang, et al., Effects on IL-1β signaling activation induced by water and organic extracts of fine particulate matter ($PM_{2.5}$) in vitro, Environ. Pollut. 237 (2018) 592–600.
[52] A.K. Bølling, J. Ovrevik, J.T. Samuelsen, J.A. Holme, K.E. Rakkestad, G.H. Mathisen, et al., Mono-2-ethylhexylphthalate (MEHP) induces TNF-alpha release and macrophage differentiation through different signalling pathways in RAW264.7 cells, Toxicol. Lett. 209 (1) (2012) 43–50.
[53] J. Pi, T. Li, J. Liu, X. Su, R. Wang, F. Yang, et al., Detection of lipopolysaccharide induced inflammatory responses in RAW264.7 macrophages using atomic force microscope, Micron 65 (2014) 1–9.
[54] S.Y. Park, E.M. Choi, K.S. Suh, H.S. Kim, S.O. Chin, S.Y. Rhee, et al., Tetrabromobisphenol A promotes the osteoclastogenesis of RAW264.7 cells induced by receptor activator of NF-kappa B ligand in vitro, J. Kor. Med. Sci. 34 (41) (2019) e267.
[55] M. Geiser, B. Rothen-Rutishauser, N. Kapp, S. Schurch, W. Kreyling, H. Schulz, et al., Ultrafine particles cross cellular membranes by nonphagocytic mechanisms in lungs and in cultured cells, Environ. Health Perspect. 113 (11) (2005) 1555–1560.
[56] H. Yue, W. Wei, Z. Yue, P. Lv, L. Wang, G. Ma, et al., Particle size affects the cellular response in macrophages, Eur. J. Pharmaceut. Sci. 41 (5) (2010) 650–657.
[57] Q. Wang, Y. Liu, H. Wang, P. Jiang, W. Qian, M. You, et al., Graphdiyne oxide nanosheets display selective anti-leukemia efficacy against DNMT3A-mutant AML cells, Nat. Commun. 13 (1) (2022) 5657.
[58] A.G. Dupuy, E. Caron, Integrin-dependent phagocytosis: spreading from microadhesion to new concepts, J. Cell Sci. 121 (11) (2008) 1773–1783.
[59] J. Sarkar, X. Wen, E.J. Simanian, M.L. Paine, V-type ATPase proton pump expression during enamel formation, Matrix Biol. 52–54 (2016) 234–245.
[60] R.S. Lacruz, S.J. Brookes, X. Wen, J.M. Jimenez, S. Vikman, P. Hu, et al., Adaptor protein complex 2-mediated, clathrin-dependent endocytosis, and related gene activities, are a prominent feature during maturation stage amelogenesis, J. Bone Miner. Res. 28 (3) (2013) 672–687.
[61] J. El-Benna, P.M. Dang, M.A. Gougerot-Pocidalo, J.C. Marie, F. Braut-Boucher, p47phox, the phagocyte NADPH oxidase/NOX2 organizer: structure, phosphorylation and implication in diseases, Exp. Mol. Med. 41 (4) (2009) 217–225.
[62] I. Dahan, E. Pick, Strategies for identifying synthetic peptides to act as inhibitors of NADPH oxidases, or "all that you did and did not want to know about Nox inhibitory peptides", Cell. Mol. Life Sci. 69 (14) (2012) 2283–2305.
[63] A. Turchinovich, A.G. Tonevitsky, B. Burwinkel, Extracellular miRNA: a collision of two paradigms, Trends Biochem. Sci. 41 (10) (2016) 883–892.
[64] M.R. Tumolo, A. Panico, A. De Donno, P. Mincarone, C.G. Leo, R. Guarino, et al., The expression of microRNAs and exposure to environmental contaminants related to human health: a review, Int. J. Environ. Health Res. 32 (2) (2020) 332–354.
[65] J.M. Austyn, S. Gordon, F4/80, a monoclonal antibody directed specifically against the mouse macrophage, Eur. J. Immunol. 11 (1981) 805–815.
[66] M.P. Ramprasad, W. Fischer, J.L. Witztum, G.R. Sambrano, O. Quehenberger, D. Steinberg, The 94- to 97-kDa mouse macrophage membrane protein that recognizes oxidized low density lipoprotein and phosphatidylserine-rich liposomes is identical to macrosialin, the mouse homologue of human CD68, Proc. Natl. Acad. Sci. U.S.A. 92 (1995) 9580–9584.
[67] J. Ma, X. Liu, Y. Yang, J. Qiu, Z. Dong, Q. Ren, et al., Binding of benzo[a]pyrene alters the bioreactivity of fine biochar particles toward macrophages leading to deregulated macrophagic defense and autophagy, ACS Nano 15 (6) (2021) 9717–9731.